Research Square

Preprints are preliminary reports that have not undergone peer review.
They should not be considered conclusive, used to inform clinical practice,
or referenced by the media as validated information.

Urea-induced acidification drives bacterial succession and hysteretic metal mobilization in a wheat-peanut rotation soil system in China

Lu Xia
Shandong University of Science and Technology
Tao Liu
Shandong University of Science and Technology
Bin Li
Luchuan County Agricultural Technology Extension Station
Jie Chen
Shandong University of Science and Technology
Mengjie Qin
Shandong University of Science and Technology
Haohao Cui
cuihao20261023@163.com

Chinese Academy of Geological Sciences
Fengxin Kang
Shandong University of Science and Technology

Research Article

Keywords: Soil acidification, Urea application, Heavy metal mobilization, Bacterial community succession, Nitrification

Posted Date: November 16th, 2026

DOI: https://doi.org/10.21203/rs.3.rs-11601119/v1

License: This work is licensed under a Creative Commons Attribution 4.0 International License.
Read Full License

Additional Declarations: No competing interests reported.

Urea-induced acidification drives bacterial succession and hysteretic metal mobilization in a wheat-peanut rotation soil system in China

Lu Xia [a], Tao Liu [a], Bin Li [b], Jie Chen [a], Mengjie Qin [a], Haohao Cui [c, *], Fengxin Kang [a, *]

[a] Shandong Key Laboratory of Geothermal Clean Energy, College of Earth Science and Engineering, Shandong University of Science and Technology, Qingdao 266590, China

[b] Luchuan County Agricultural Technology Extension Station, Yulin 537000, China

[c] Institute of Hydrogeology and Environmental Geology, Chinese Academy of Geological Sciences, Shijiazhuang 050061, China

[*] Corresponding author.

E-mail address: cuihao924@126.com

Abstract

Excessive nitrogen fertilization is a primary driver of farmland soil acidification, yet the dose-dependent coupling among acidification, heavy metal mobilization, and microbial community succession remains poorly resolved. In this study, a 60-day aerobic incubation of a wheat-peanut rotation soil amended with urea at 0, 100, 300, and 500 μg/g dry weight soil, integrating soil physicochemical analysis, DTPA-extractable metal monitoring, 16S rRNA amplicon sequencing, and FAPROTAX functional prediction. Soil pH declined to its minimum on day 28, with reductions increasing with urea rate, and recovery by day 60 was limited and negatively correlated with nitrogen input. NH_4^+-N peaked on day 14 and remained elevated under high nitrogen, whereas a transient NO_2^--N pulse coincided with the pH minimum, confirming nitrification as the dominant proton-producing pathway. Notably, Urea300 and Urea500 reached comparable NH_4^+ and NO_3^- levels despite differing inputs, indicating disproportionately active nitrification at the intermediate dose. Heavy metal mobilization exhibited a pronounced hysteresis: pH reached its minimum on day 28, whereas Cd, Cu, and Zn mobilization peaked on day 60—a lag of approximately one month—decoupling metal toxicity from pH recovery, although all metals remained below GB 15618-2018 thresholds. For bacterial communities, Urea100 had minimal effects, Urea300 triggered drastic functional reorganization (nitrification and manganese oxidation increased; aerobic chemo-heterotrophy halved; nitrogen fixation and hydrocarbon degradation nearly lost), and Urea500 exhibited partial functional recovery and greater stability, reflecting rebalancing rather than a simple dose-dependent decline. These shifts were tightly coupled with taxonomic reorganization, with *Gammaproteobacteria* and its representative genus *Chujaibacter* driving enhanced nitrification,

while *Alphaproteobacteria* and *Sphingomonas* showed inverse trends. These findings reveal a nonlinear, threshold-like response of soil microbial communities to nitrogen-induced acidification and highlight the need to control single urea applications below 300 kg N/ha with intervals of no less than 60 days to safeguard soil ecological health.

Keywords: Soil acidification; Urea application; Heavy metal mobilization; Bacterial community succession; Nitrification

1. Introduction

Global food security remains critically dependent on soil resources, with approximately 98.8% of human caloric intake being derived either directly or indirectly from soil (Kraamwinkel et al., 2021; Van Vuuren et al., 2025). However, this foundational resource is undergoing progressive degradation via soil acidification, the ecological risks of which are increasingly approaching planetary boundary thresholds (FAO and ITPS, 2015). Soil acidification, broadly defined as a sustained decline in soil pH, has emerged as a major constraint on global agricultural productivity, adversely affecting crop growth, yield stability, and produce quality. In China, the combined pressures of long-term excessive nitrogen (N) fertilization and continuous base cation removal through crop harvesting have reduced the average pH of arable soils by 0.12 ~ 0.80 units over recent decades (Dai et al., 2017). The detrimental consequences of soil acidification are multifaceted. On one hand, elevated proton (H^+) activity reduces the availability of essential nutrients, such as phosphorus (P), calcium (Ca), and magnesium (Mg), thereby limiting crop nutrient uptake (Holland et al., 2019). On the other hand, acidification promotes the mobilization and activation of potential toxic metals, including iron (Fe), manganese (Mn), zinc (Zn), and cadmium (Cd), thus increasing the risk of heavy metal phytotoxicity and food-chain transfer (Dong et al., 2022). Furthermore, shifts in soil pH profoundly alter the composition, diversity, and functional potential of soil microbial communities (Duan et al., 2025; Qu et al., 2024; Wang et al., 2022), which in turn modulate microbially driven elemental cycling processes, including C and N transformations (Fierer and Jackson, 2006; Shen et al., 2013).

Nitrogen fertilizer is widely recognized as a primary anthropogenic driver of farmland soil

acidification. Long-term field trials have demonstrated that acidifying effect varies substantially among different N fertilizer forms (Frey et al., 2004; Meng et al., 2019). Among these, ammonium-based N derived from urea hydrolysis, following by nitrification, represents a major source of H^+ release, constituting a dominant pathway for the progressive acidification of cultivated soils (Guo et al., 2010). Despite this established linkage, several critical knowledge gaps remain. First, the majority of previous studies have adopted a binary experimental design (i.e., a single fertilization rate vs. a non-fertilized control), which is inherently insufficient to capture the dose-dependent response patterns of soil physicochemical properties and microbial communities to graded urea inputs. In acid agricultural ecosystems, the relationship between N application rate and acidification intensity is unlikely to be linear (Wang et al., 2026); rather, a critical threshold may exist beyond which acidification accelerates disproportionately. However, this dose-response relationship and the potential threshold behavior remain inadequately characterized in the current literatures. Second, the dynamic coupling among soil acidification, heavy metal mobilization, and microbial community succession has yet to be fully elucidated. Most investigations have focused on binary associations (e.g., acidification and community, or metals and community) (Morrison et al., 2016), and few have simultaneously tracked the co-evolution of soil physicochemical parameters and microbial assemblages within a unified experimental framework remains scarce (Dror et al., 2017). Third, the mechanisms underlying the persistence of N cycling functions under extreme acidification remains obscure. Classical autotrophic nitrifiers exhibit an optimal pH above 7.0, when soil pH drops below 4.0, the activity of canonical nitrification pathways is severely inhibited (Wang et al., 2023). Nevertheless, soil N cycling may not necessarily be interrupted under such conditions

(Kyveryga et al., 2004), suggesting the existence of alternative (e.g., heterotrophic or acid-tolerant) pathways that sustain ammonia oxidation. Elucidating these maintenance mechanisms is of fundamental importance for understanding soil N biogeochemistry under acid stress and for predicting ecosystem responses to ongoing acidification.

To address the above gaps, the present study selected soils from a representative wheat-peanut rotation system in the Nanyang Basin, Henan Province, China. A gradient urea-addition (0, 100, 300, and 500 μg urea/g dry weight soil) experiment was established, and a 60-day incubation was conducted with repeated sampling at multiple time intervals. A suite of soil physicochemical variables was monitored, including soil pH, organic carbon content (SOC), inorganic N fractions (NH_4^+-N, NO_3^--N, and NO_2^--N), and soluble heavy metal concentrations. Concurrently, 16S rRNA high-throughput sequencing was employed to comprehensively characterize soil bacterial community composition and temporal succession. The objectives of this study were to: (i) characterize the acidification process under varying urea application rates and to evaluate their driving effects on key physicochemical properties; (ii) elucidate the response patterns of soluble heavy metal mobility to urea-induced acidification; and (iii) disentangle the coupling relationships between bacterial community succession and shifts in the soil chemical environment. The findings are expected to provide a scientific foundation for optimizing N fertilizer management and sustaining soil health in intensive agricultural systems.

2. Materials and methods

2.1 Study area and sampling

The study area is situated in the alluvial plain of Fangcheng County, Nanyang City, Henan Province, China. The region is characterized by a warm-temperate continental monsoon climate,

with a mean annual temperature of approximately 14.9 °C and a mean annual precipitation of approximately 800 mm. The dominant land use is a wheat-peanut rotation system, which is representative of intensive farming practices in the North China Plain.

Soil samples were collected from the cultivated horizon (0 ~ 20 cm depth) using a four-point sampling strategy, with adjacent sampling points spaced approximately 50 m apart. Visible plant residues, including roots and aboveground litter were carefully removed from the surface (without scraping off the humic surface layer), and the four subsamples were thoroughly homogenized to obtain a composite sample. The composite soil was air-dried at ambient temperature, gently ground, and sieved through a 2 mm mesh prior to further use.

2.2 Experimental design

For the incubation experiment, aliquots of 200 g (calculated on an oven-dry equivalent basis) of the sieved soil were placed into 500 mL polyethylene bottles and subjected to aerobic incubation under controlled conditions. Urea was added at three rates of 100, 300, and 500 μg/g dry weight soil, designated as Urea100, Urea300, and Urea500, respectively. A control treatment without urea addition (CS) was established. Meanwhile, a subsample of the original, unincubated soil was retained and designated as OS. All treatments were performed in triplicate.

All incubation bottles were maintained at 25 °C in the dark for 60 days. The bottle openings were covered with gas-permeable membranes to ensure aerobic conditions while minimizing evaporative water loss. Throughout the incubation period, soil moisture was maintained at approximately 35% of field water-holding capacity by periodically supplying deionized water based on gravimetric adjustment. Sampling was conducted at days 0, 7, 14, 28, and 60, and the collected subsamples were analyzed for soil pH, SOC, NH_4^+-N, NO_3^--N, NO_2^--N, and

diethylenetriaminepentaacetic acid (DTPA)-extractable Fe, Cu, Cd, and Zn concentrations. For microbial community analysis, soil samples from the CS, Urea100, Urea300, and Urea500 treatments were collected on days 14 and 28 and analyzed via 16S rRNA high-throughput sequencing to profile bacterial abundance, composition, and functional groups in response to graded urea inputs. To assess temporal successional patterns, samples from all treatments collected on the same day were pooled and marked as Urea-14 (day 14), and Urea-28 (day 28), representing the integrated community successional states at mid- and late-incubation stages.

2.3 Analytical methods

2.3.1 Soil physicochemical properties

Soil pH was determined potentiometrically following the ISO 10390:2024 standard (ISO, 2024), using a soil-to-water ratio of 5:1 (m/V). The suspension was equilibrated, and the pH value was measured with a calibrated pH meter (HQ40d, HACH, USA). Soil inorganic nitrogen fractions (NH_4^+-N, NO_3^--N, NO_2^--N) were extracted with potassium chloride solution and quantified by ultraviolet-visible spectrophotometry (UV-2802, UNICOSH, China). Soil organic carbon (SOC) content was determined by the potassium dichromate oxidation-external heating titration method with titration. Available fractions of Fe, Cu, Cd, and Zn were extracted using DTPA solution, and the concentrations in the extracts were measured by flame atomic absorption spectrophotometry (TAS-986F, pgeneral, China).

2.3.2 Bacterial DNA extraction and high-throughput sequencing

Total genomic DNA was extracted from each sample using a commercial DNA extraction kit (FastDNA® SPIN Kit for Soil, MP Biomedicals) following the manufacturer's protocols. DNA quality and integrity were verified by 1% agarose gel electrophoresis. The V3-V4 hypervariable

regions of the bacterial 16S rRNA gene were amplified using the barcoded universal primer pair 338F (5′-ACTCCTACGGGAGGCAGCAG-3′) and 806R (5′-GGACTACHVGGGTWTCTAAT-3′). PCR amplifications were performed with TransStart FastPfu DNA Polymerase (TransGen, AP221-02) on an ABI GeneAmp® 9700 thermal cycler. The PCR products were separated by 2% agarose gel electrophoresis, and the target bands were excised and purified using the AxyPrep DNA Gel Extraction Kit (Axygen). Purified amplicons were quantified with the QuantiFluor™-ST blue fluorescence quantification system (Promega), and equimolar amounts of each sample were pooled. Sequencing libraries were constructed following the TruSeq™ DNA Sample Prep Kit protocol and subjected to paired-end sequencing (2 × 300 bp) on the Illumina MiSeq platform.

2.3.3 Bioinformatics analysis

Raw sequencing reads were quality-filtered using Fastp (v0.20.0). Reads containing adapter sequences, more than three consecutive low-quality bases ($Q < 20$), a proportion of ambiguous bases (N) exceeding 10%, or a final length of less than 50 bp were discarded. The resulting high-quality paired-end reads were assembled into full-length amplicon using FLASH (v1.2.11) with the following parameters: minimum overlap ≥ 10 bp and maximum mismatch rate < 0.2. The assembled sequences were subsequently denoised, dereplicated, and chimera-filtered using the DADA2 algorithm implemented in the QIIME2 platform, generating amplicon sequence variant (ASV) representative sequences and an ASV feature abundance table.

Taxonomic assignment of ASVs was performed using the RDP Classifier (confidence threshold ≥ 0.7) against the SILVA 16S rRNA gene database (v138). Sequences annotated as Chloroplast or Mitochondria were removed from subsequent analyses. After rarefying to the

minimum sequencing depth across all samples, the following analyses were conducted: (i) alpha diversity, assessed by the Chao1 richness index, Simpson index, and Pielou-e evenness index; (ii) beta diversity evaluated via principal coordinate analysis (PCoA) based on Bray-Curtis dissimilarity matrices, with statistical significance tested by permutational multivariate analysis of variance (PERMANOVA); and (iii) functional annotation, performed using the FAPROTAX database (v1.2.6) to obtain the ecological functional group abundance matrix for each sample.

2.4 Data processing and statistical analysis

All physicochemical parameters and bacterial alpha diversity indices are expressed as mean ± standard deviation (mean ± SD, $n = 3$). Differences in bacterial alpha diversity indices among treatments were evaluated by one-way analysis of variance (ANOVA), with statistical significance $p < 0.05$. When significant overall differences were detected among groups, post hoc multiple comparisons were performed using the least significant difference (LSD) and Duncan's multiple range tests to identify specific group differences. All ANOVA and significance tests were conducted in SPSS (IBM Corp., Armonk, NY, USA; 31.0.0), and all figures were prepared using Origin (Origin Lab Corporation, Northampton, MA, USA; v 2024b) and Adobe Illustrator (Adobe Inc., San Jose, CA, USA; v 28.4.1).

3. Results

3.1 Effects of urea application on soil pH and inorganic nitrogen fractions

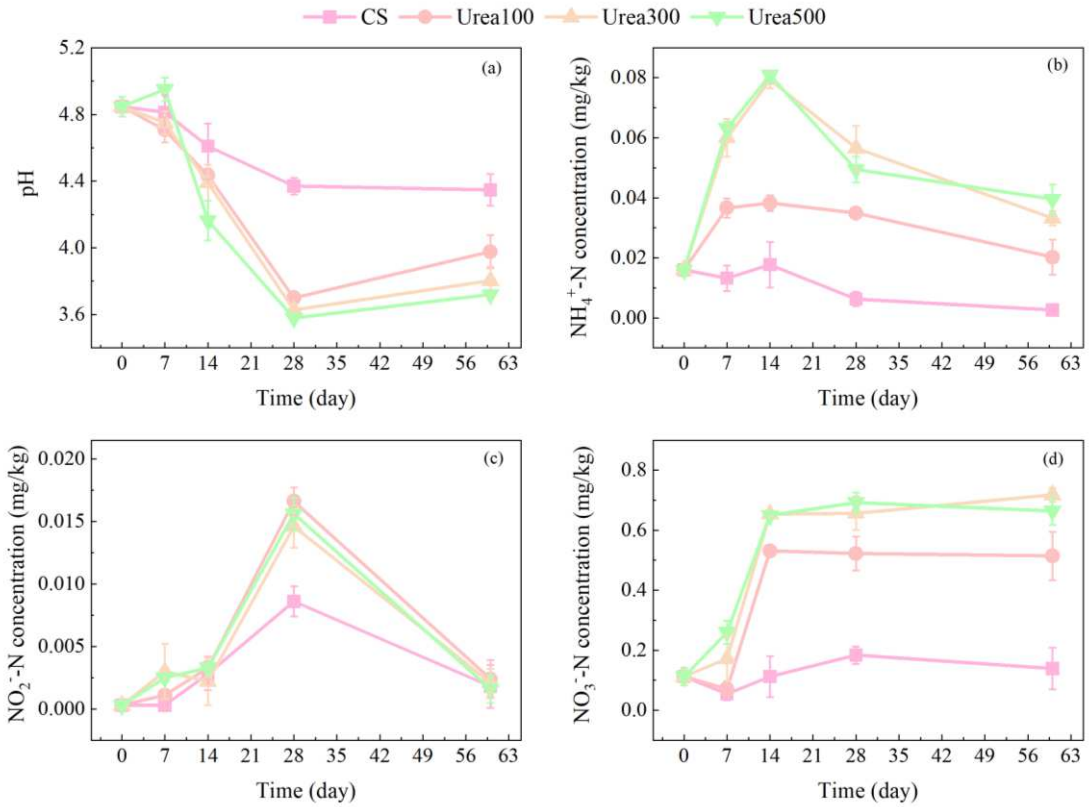


Fig. 1. Effects of urea application rate on the temporal evolution of soil pH and inorganic nitrogen fractions (NH_4^+-N, NO_3^--N, NO_2^--N) during a 60-day incubation. (a) Soil pH; (b) NH_4^+-N concentration; (c) NO_2^--N concentration; (d) NO_3^--N concentration. Data are presented as means ± SD (n = 3).

The temporal changes in soil pH under different urea application rates are presented in Fig. 1a. Over the 60-day incubation, soil pH in all treatments exhibited a consistent pattern of an initial sharp decline followed by a modest recovery, with the magnitude of acidification and the subsequent rebound varying markedly among urea addition levels. At the early stage (day 7), soil pH in all treatments remained close to the initial value (4.85 ± 0.06), with the CS group at 4.81 ± 0.10, and the Urea100, Urea300, and Urea500 groups at 4.71 ± 0.08, 4.75 ± 0.07, and 4.95 ± 0.07, respectively, indicating that the alkalinity generated by urea hydrolysis (Kyveryga

et al., 2004; Wang et al., 2023) and the acidity produced by nitrification were approximately balanced during this period. By day 28, soil pH in all treatments reached the lowest values over the entire incubation. The CS group declined to 4.37 ± 0.05, whereas Urea100, Urea300, and Urea500 decreased markedly to 3.70 ± 0.01, 3.63 ± 0.03, and 3.58 ± 0.02, representing reductions of 9.9%, 23.7%, 25.2%, and 26.2% from the initial pH (4.85 ± 0.06), respectively. This pronounced dose-dependent response indicated that elevated urea inputs intensify soil acidification, with higher N rates corresponding to progressively greater pH declines. At the later stage (day 60), pH in all urea-treated groups recovered to varying extents, with Urea100, Urea300, and Urea500 rising to 3.97 ± 0.10, 3.80 ± 0.08, and 3.72 ± 0.01, corresponding to recovery amplitudes of 7.3%, 4.7%, and 3.9%, respectively. In contrast, the CS group continued to decline slightly to 4.25 ± 0.03. Although partial recovery, pH in all treatment groups remained substantial below the initial level (4.85 ± 0.06). These results revealed that a negative correlation between urea application rate and pH recovery amplitude, suggesting that higher nitrogen inputs not only intensify initial acidification but also compromise the soil's buffering capacity and resilience, leading to more persistent and less reversible acidification.

Fig. 1b shows the temporal variations in NH_4^+-N concentration under different urea application rates. In the CS group, NH_4^+-N concentration exhibited a steady decline over time, from an initial value of 0.016 ± 0.002 to 0.003 ± 0.001 mg/kg by day 60, reflecting the gradual depletion of native mineral nitrogen through microbial assimilation or nitrification. However, all urea-treated groups displayed a distinct pattern. Specifically, NH_4^+-N concentrations reached to maximum values of 0.038 ± 0.026, 0.079 ± 0.003, and 0.081 ± 0.0005 mg/kg in Urea100, Urea300, and Urea500, respectively. Subsequently, it gradually decreased to 0.020 ± 0.026,

224 0.033 ± 0.002, and 0.040 ± 0.005 mg/kg by day 60. Notably, although the temporal trends were
225 qualitatively similar across urea treatments, the magnitude of NH_4^+-N accumulation differed.
226 At the peak, NH_4^+-N concentrations in Urea300 and Urea500 were approximately twice that of
227 Urea100. By day 60, Urea300 and Urea500 still maintained levels 1.5 ~ 2 times higher than
228 Urea100. This implied that higher urea inputs led to greater NH_4^+-N release from hydrolysis,
229 and that under high urea addition, substantial residual NH_4^+-N persist even after 60 days,
230 suggesting that nitrification capacity may become constrained or saturated, limiting the
231 conversion of NH_4^+-N to NO_3^--N.

232 Nitrite nitrogen (NO_2^--N) is a reactive intermediate in the sequential oxidation of NH_4^+-N to
233 NO_3^--N (Ren et al., 2026). Due to its high chemical reactivity and rapid turnover, NO_2^--N
234 typically does not accumulate to appreciable concentrations in natural soils. In this study,
235 NO_2^--N exhibited a transient accumulation exclusively on day 28 across all treatments (Fig. 1c),
236 reaching 0.017 ± 0.001, 0.015 ± 0.002, and 0.016 ± 0.001 mg/kg in Urea100, Urea300, and
237 Urea500, respectively—approximately 1.7 ~ 1.9 times that of the CS group (0.009 ± 0.001
238 mg/kg). This indicated that the rate of NH_4^+-N oxidation to NO_2^--N temporarily exceeded the
239 rate of NO_2^--N oxidation to NO_3^--N, creating a transient "bottleneck" in the nitrification
240 sequence. The synchronous occurrence of this NO_2^--N peak with the pH minimum on day 28
241 (Fig. 1a) further supported the conclusion that nitrification was the dominant process driving
242 soil acidification.

243 The temporal dynamics of NO_3^--N concentrations are illustrated in Fig. 1d. Following urea
244 addition, NO_3^--N exhibited a pattern of a rapid accumulation followed by relative stabilization.
245 The initial background NO_3^--N was 0.112 ± 0.029 mg/kg. By day 7, NO_3^--N in Urea100

decreased slightly to 0.071 ± 0.026 mg/kg; comparatively, in the medium- and high-rate treatments (Urea300 and Urea500), it increased to 0.172 ± 0.075 and 0.260 ± 0.039 mg/kg, respectively. This early divergence implied that medium to high urea inputs provided sufficient substrate for initiate nitrification preferentially, while low-rate urea addition exerted a marginal or lagged effect. By day 14, NO_3^--N in all urea-treated groups increased substantially and reached maximum values of 0.531 ± 0.017 (Urea100), 0.653 ± 0.009 (Urea300), and 0.649 ± 0.012 (Urea500) mg/kg, approximately 4.7~5.8 times that of the CS group (0.112 ± 0.068 mg/kg). Thereafter, NO_3^--N remained relatively stable through day 60, with final values of 0.514 ± 0.081, 0.717 ± 0.023, and 0.664 ± 0.046 mg/kg, respectively. This stable plateau suggested that once nitrification was fully established, NO_3^--N production and consumption reached a dynamic equilibrium.

Notably, the temporal variations in NO_3^--N and NH_4^+-N in Urea300 and Urea500 were broadly similar throughout the incubation, implying that once the urea addition exceeded a certain threshold, the accumulation of nitrification products may have been constrained by the oxidative capacity of the nitrifying community or electron acceptor availability, rather than being governed solely by NH_4^+-N substrate concentration. In the CS group, NO_3^--N fluctuated within a narrow range (0.054 ± 0.029 to 0.183 ± 0.029 mg/kg), confirming that native soil nitrification was negligible in the absence of exogenous nitrogen input.

3.2 Dynamics of soil extractable heavy metal contents

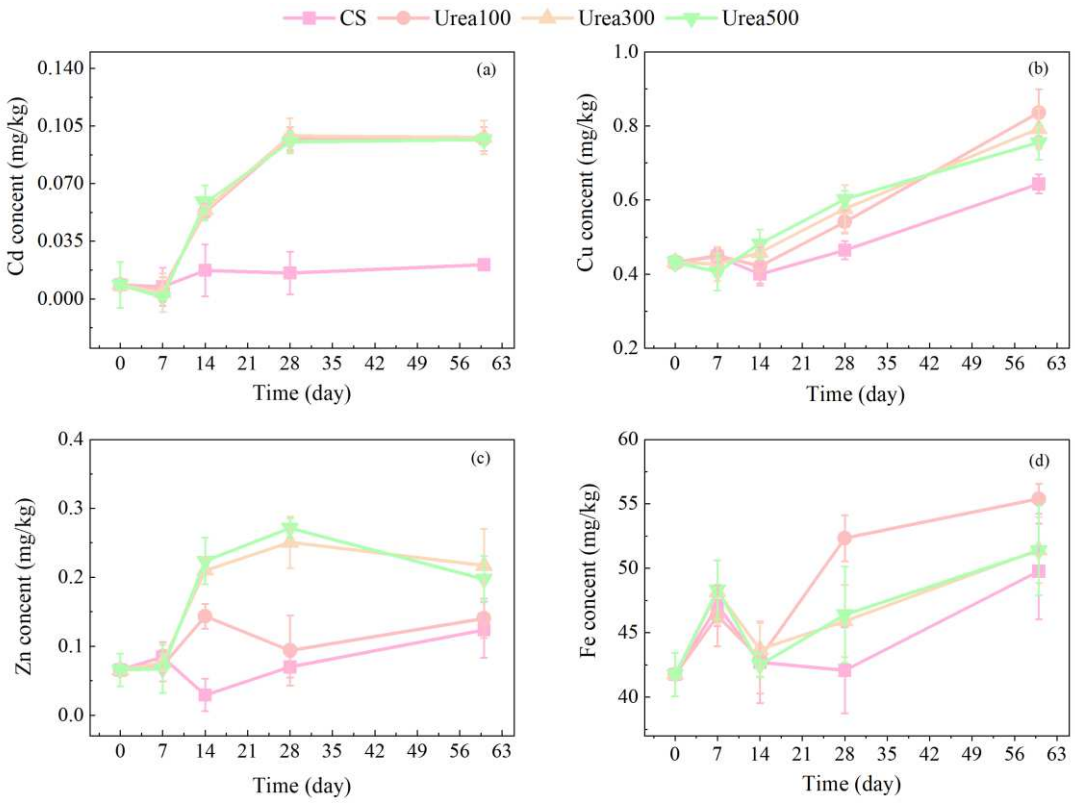


Fig. 2. Temporal dynamics of soil extractable Cd, Cu, Zn, and Fe contents under different urea application rates over a 60-day incubation period. (a) Cd; (b) Cu; (c) Zn; (d) Fe. Data are presented as means ± SD (n = 3).

The temporal dynamics of soil extractable Cd, Cu, Zn, and Fe contents under different urea addition levels are presented in Fig. 2. As shown in Fig. 2a, the initial soil extractable Cd content was 0.0085 ± 0.014 mg/kg. During the first 7 days, Cd concentrations remained relatively low across all treatments, with no discernible treat effect. From day 14 onward, however, Cd in the urea-treated groups increased substantially, reaching 0.0527 ± 0.005, 0.054 ± 0.002 and 0.0583 ± 0.011 mg/kg in Urea100, Urea300, and Urea500, respectively. By day 28, Cd concentrations in all urea treatments levelled off at 0.10 ± 0.007, 0.098 ± 0.102 and 0.097 ± 0.003 mg/kg, respectively, with no clear dose-dependent differentiation among different urea addition levels.

Notably, all values remained below the risk control standard for agricultural soils (0.3 mg/kg) stipulated in the Chinese national standard (GB 15618-2018). In contrast, the CS group maintained consistently low Cd concentrations throughout the incubation, with a final value of only 0.021 mg/kg on day 60, highlighting the critical role of urea-induced acidification in mobilizing soil Cd.

Fig. 2b displays the temporal changes in soil Cu content. The initial Cu content was 0.432 ± 0.019 mg/kg. By day 14, Cu concentrations in the urea-treated groups began to rise gradually, with values of 0.421 ± 0.052 (Urea100), 0.458 ± 0.018 (Urea300), and 0.482 ± 0.038 mg/kg (Urea500), compared with 0.400 ± 0.026 mg/kg in the Cs group. Thereafter, Cu content continued to increase progressively throughout the remaining incubation period, reaching the highest levels on day 60 in all treatment groups: 0.836 ± 0.063 (Urea100), 0.793 ± 0.055 (Urea300), and 0.756 ± 0.048 mg/kg (Urea500), all exceeding the CS group (0.644 ± 0.026 mg/kg). Interestingly, the highest Cu concentration was observed in the Urea100 rather than the high-dose treatments, suggesting that Cu mobilization may be influenced by factors beyond simple pH decline, such as competitive interactions with other cations or changes in organic matter complexation. All measured Cu concentrations remained far below the risk control threshold for agricultural soils (50 mg/kg) specified in the Chinese national standard (GB 15618-2018).

As for Zn content, the initial concentration was 0.065 ± 0.024 mg/kg. During the first 7 days, no clear trend was observed across treatments. By day 14, however, Zn concentrations increased markedly in a dose-dependent manner, reaching 0.143 ± 0.018 (Urea100), 0.210 ± 0.020 (Urea300), and 0.224 ± 0.034 mg/kg (Urea500), compared with only 0.029 ± 0.023 mg/kg in

the CS group—a striking contrast indicating that urea addition triggered substantial Zn mobilization. On day 28, Zn concentrations in Urea300 and Urea500 reached to the maximum values of 0.251 ± 0.037 and 0.271 ± 0.014 mg/kg, respectively, approximately 3 times that of the CS group (0.070 ± 0.015 mg/kg). By day 60, the patterns diverged: Zn concentration in Urea100 continued to rise to 0.140 ± 0.028 mg/kg, whereas that in Urea300 and Urea500 declined from their peaks to 0.251 ± 0.037 and 0.271 ± 0.014 mg/kg, respectively, though still remaining substantially higher than in the CS group (0.124 ± 0.041 mg/kg). This late-stage decline in the high-dose treatments may reflect precipitation of Zn under prolonged acidification, possibly mediated by the concurrent increase in Fe/Mn oxide surfaces (Fig. 2d) or changes in microbial activity that influence metal speciation. Overall, Zn mobilization exhibited a clear dose-dependent pattern, with higher urea addition generally leading to higher Zn concentrations.

The initial Fe content was 41.758 ± 1.679 mg/kg (Fig. 2d). On day 7, Fe concentrations remained similar across all treatments (ranging from 46.324 ± 2.390 to 48.338 ± 2.273 mg/kg in urea groups, vs. 47.107 ± 1.595 mg/kg in CS), indicating that urea addition exerted no significant effect on Fe mobilization during the early incubation phase. Over prolonged incubation, Fe content exhibited a V-shaped pattern across all treatments—first decreasing and then increasing. By day 14, Fe concentrations fell back to levels close to the initial values (ranging from 42.497 ± 0.938 to 43.706 ± 2.098 mg/kg across urea treatments, vs. 42.700 ± 3.159 mg/kg in CS). Thereafter, Fe content increased continuously, reaching peak levels on day 60 in all urea-treated groups (55.392 ± 1.147, 51.418 ± 2.565, and 51.376 ± 3.476 mg/kg in Urea100, Urea300, and Urea500, respectively), all higher than the CS group (49.765 ± 3.713

mg/kg). This result indicated that urea-induced soil acidification promoted Fe mobilization to a certain extent, likely through enhanced dissolution of Fe-bearing minerals and reductive dissolution processes. Notably, the highest Fe concentration was observed in the Urea100 rather than the high-dose groups, mirroring the pattern seen for Cu, which may reflect the interplay between acidification intensity and the availability of Fe-bearing phases, or the formation of secondary Fe precipitates under extremely low pH conditions that reduce extractability.

3.3 Bacterial community characteristics

3.3.1 Alpha diversity

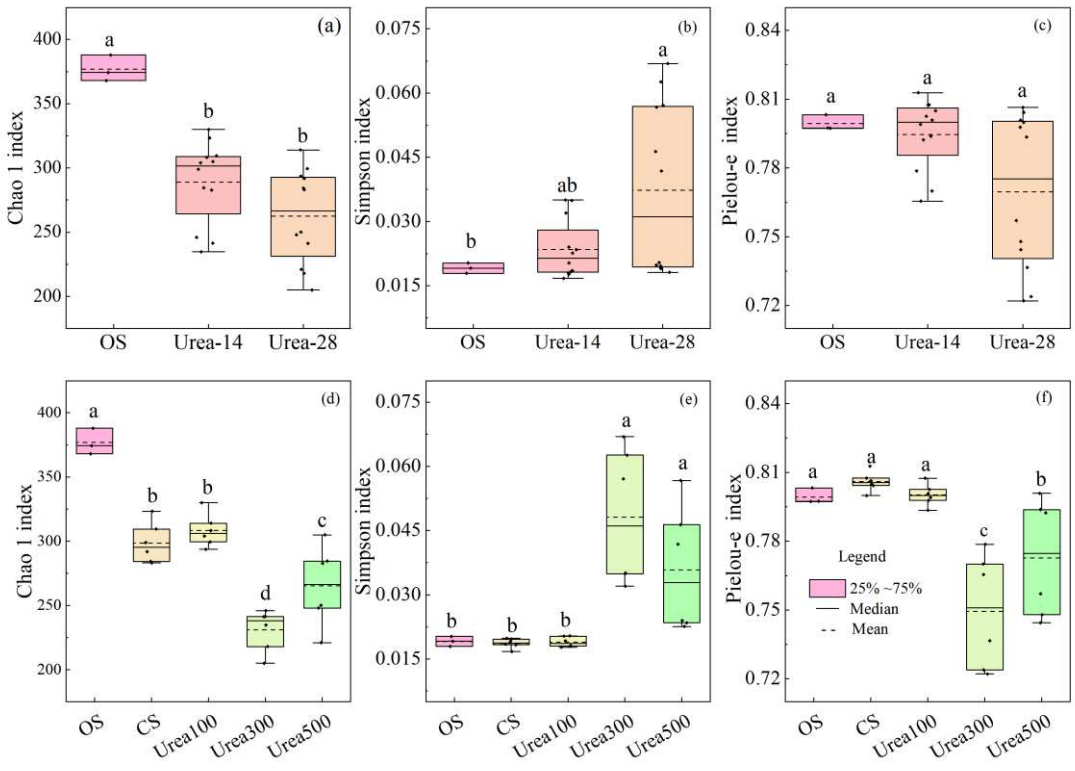


Fig. 3. Responses of soil bacterial alpha diversity indices (Chao1, Simpson, and Pielou-e) to different urea application rates and incubation time. (a-c) Temporal variation of (a) Chao1, (b) Simpson, and (c) Pielou-e indices across incubation stages (OS, Urea-14, Urea-28); (d-f) Dose-dependent variation of (d) Chao1, (e) Simpson, and (f) Pielou-e indices across urea

addition levels (OS, CS, Urea100, Urea300, Urea500). In each boxplot, the solid and dashed horizontal lines denote the median and mean values, respectively. Different lowercase letters above the boxes indicate significant differences among treatments at $p < 0.05$ (one-way ANOVA followed by post hoc test). Individual data points represent biological replicates ($n = 3$).

The responses of soil bacterial alpha diversity indices (Chao1, Simpson, and Pielou-e) to different urea application rates and incubation durations are presented in Fig. 3. Figs. 3(a-c) illustrates the temporal changes in bacterial community alpha diversity across different incubation stages. The Chao1 richness index (Fig. 3a) revealed that compared with the original soil (OS: 376 ± 10), the values for Urea-14 (289 ± 32) and Urea-28 (262 ± 36) were significantly lower ($p < 0.05$), indicating that a substantial proportion of bacterial taxa incapable of acclimating to elevated nitrogen conditions were eliminated shortly after urea addition. No significant difference was observed between Urea-14 and Urea-28, suggesting that the major loss of species richness occurred within the first 14 days, after which the community reached a relatively stable. The Simpson dominance index (Fig. 3b) exhibited a similar trend, with the OS group being significantly lower than both urea-treated groups ($p < 0.05$), implying that urea addition reduced overall community diversity and promoted a more simplified, dominance-skewed community structure. Notably, the Urea-28 group displayed a wider interquartile range than Urea-14, indicating increased heterogeneity among replicates in terms of dominance concentration at later incubation stages. The Pielou-e evenness index (Fig. 3c) further corroborated these patterns, declining from 0.80 ± 0.00 in the OS group to 0.77 ± 0.03 in Urea-28, reflecting a progressive loss of community evenness over time. Collectively, the three

indices demonstrated that urea application impose a strong environmental filter: taxa intolerant to high nitrogen or acidified conditions were gradually eliminated, and among the surviving populations, differential stress tolerance led to a disproportionate dominance of a few adapted taxa, ultimately resulting in reduced community diversity, evenness, and functional redundancy.

Figs. 3(d-f) further depicts the changes in alpha diversity indices across the gradient of urea application rates. The Chao1 richness index (Fig. 3d) showed that the OS group exhibited the highest value (376 ± 10), significantly exceeding all treatment groups ($p < 0.05$). The CS (298 ± 15) and Urea100 (308 ± 12) groups were not significantly different from each other, indicating that low-rate urea addition did not markedly suppress species richness. With further increases in urea rate, however, Chao1 values declined substantially to 231 ± 16 (Urea300) and 265 ± 30 (Urea500). The slight rebound observed in Urea500 relative to Urea300 may reflect the survival of a limited set of highly tolerant taxa after the elimination of sensitive groups, rather than a true recovery of diversity. The Simpson dominance index (Fig. 3e) confirmed this dose-dependent pattern: the Simpson indices for Urea300 and Urea500 were significantly higher than those for the OS, CS, and Urea100 ($p < 0.05$), indicating that under medium- and high-rate treatments, community structure became increasingly concentrated toward a few dominant species. In contrast, the Simpson indices for OS, CS, and Urea100 remained low (all means approximately 0.02) and were not significantly different from each other, underscoring the resilience of community evenness under low nitrogen input. The Pielou-e evenness index (Fig. 3f) provided further evidence of dose-induced community divergence. Evenness values for OS, CS, and Urea100 displayed no significant differences, with means maintained at 0.80-0.81. In contrast, the Pielou-e indices for Urea300 and Urea500 were significantly lower than those for

the low-rate groups ($p < 0.05$), confirming that medium- and high-rate applications severely disrupted community equitability. Overall, the results from Figs. 3(d-f) clearly demonstrated that the filtering effect of urea application on soil bacterial communities was distinctly dose-dependent. Low-rate addition (Urea100) remained within the tolerance and recovery threshold of the indigenous community, with no drastic structural reorganization; whereas medium- and high-rate treatments (Urea300 and Urea500) imposed strong environmental stress, forcing the community to rapidly converge toward acid-tolerant and high-nitrogen-tolerant dominant populations, resulting in marked structural simplification and diminished ecological functional potential.

3.3.2 Bacterial community composition

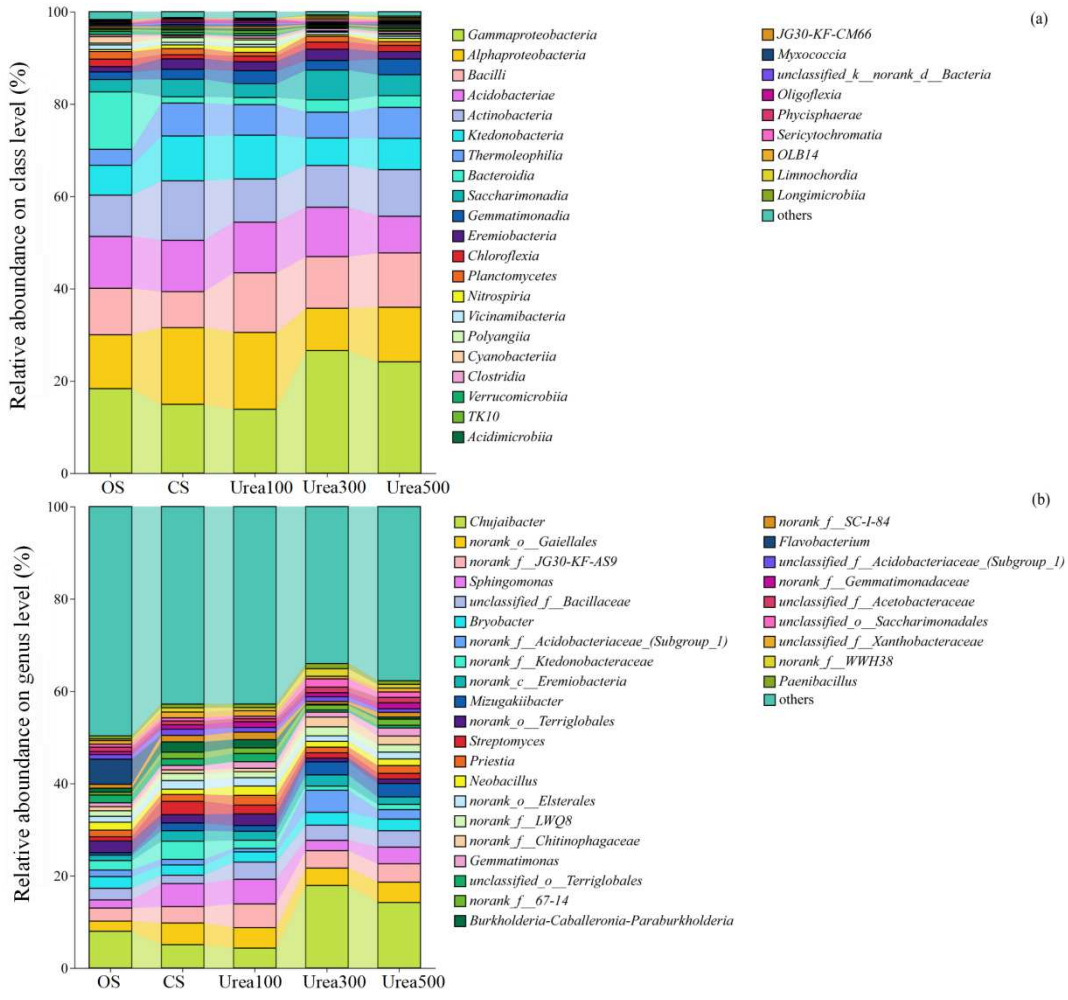


Fig. 4. Effects of urea application rates on the relative abundance of soil bacterial communities at the (a) class and (b) genus levels. Only the top 30 most abundant taxa are displayed individually; the remaining taxa were categorized into "Others".

Fig. 4(a) presents the relative abundance of soil bacterial communities at the class level (Table S1). Across all samples, *Gammaproteobacteria* (18.3%), *Alphaproteobacteria* (11.7%), and *Acidobacteriae* (12.9%) constituted the three dominant classes, collectively accounting for 42.9% of the total community relative abundance. These dominant taxa are pivotal in multiple soil ecological functions, encompassing nitrogen cycling (nitrification and nitrogen fixation), carbon cycling (organic matter decomposition), acid/osmatic tolerance metabolism, and protein hydrolysis (Morrison et al., 2016). Consequently, shits in their community structure may exert profound impacts on soil functionality. The relative abundance of the dominant class *Gammaproteobacteria* increased from 14.9% in the CS group to 26.6% and 24.1% in Urea300 and Urea500, respectively. This pronounced enrichment can be attributed to two synergistic factors. First, the NH_4^+ released from urea hydrolysis provided a substantial substrate for nitrifying members within this class. Second, the H^+ generated by nitrification caused a sharp drop in soil pH (as low as 3.58 in Urea500 on day 28), and certain members of *Gammaproteobacteria* possess strong physiological tolerance to low pH conditions (Niepceron et al., 2013), enabling them to thrive under acidification-induced selective pressure. In contrast, the relative abundance of *Alphaproteobacteria* decreased from 16.6% in the CS to 9.2% in Urea300 and 11.8% in Urea500. Previous studies have demonstrated that some members of this class are sensitive to low pH (Ren et al., 2026), with their metabolic activity being significantly inhibited under strongly acidic conditions ($pH \leq 3.58$) (Yang et al., 2020).

By comparison, *Acidobacteriae* exhibited a modest decrease from 11.1% to 10.7% in Urea300 and 10.1% in Urea500. This class harbors a large number of obligate acidophilic or acid-tolerant taxa (Bartkowska-Bekasiewicz et al., 2026), which are naturally adapted to strongly acidic environments (Guo et al., 2026).

Fig. 4(b) further displays the relative abundance of bacterial communities at the genus level (Table S2). Based on their dominance, ecological functions, and the extent of compositional changes, three genera—*Chujaibacter*, *Sphingomonas*, and *norank-f-Acidobacteriaceae-(Subgroup-1)* —were selected for further analysis. In the OS group, these three genera together accounted for 11.2% of the community, with a relatively dispersed distribution (*Chujaibacter* 8.0%, *Sphingomonas* 1.8%, *norank-f-Acidobacteriaceae-(Subgroup-1)* 1.4%). After incubation, the community composition in the CS and Urea100 groups showed no obvious changes, indicating that low-rate urea addition had a limited effect on genus-level community structure, consistent with the pattern observed at the class level. In the Urea300 treatment, *Chujaibacter* increased from 5.1% in the CS group to 17.9%, representing an approximately 2.51-fold increase and becoming the overwhelmingly dominant genus in this treatment. This enrichment is attributed to its ability to utilize NH_4^+ released from urea hydrolysis and to survive under low pH conditions (Yang et al., 2025). Meanwhile, *Sphingomonas* decreased from 5.0% in the CS to 2.8%. Although this genus is known to possess tolerance to heavy metal stress (Chen et al.,2024), its competitive advantage was apparently constrained under acidic conditions. *Norank-f-Acidobacteriaceae-(Subgroup-1)* increased from 1.4% to 4.8%, an approximately 2.43-fold increase, with complex polysaccharide degradation

as its primary metabolic pathway (Llado et al.,2016). In the Urea500 treatment, the response patterns were opposite: *Chujaibacter* declined from 17.9% in Urea300 to 14.2%; *Sphingomonas* rebounded from 2.8% to 3.6%; and *norank-f-Acidobacteriaceae-(Subgroup-1)* dropped markedly from 4.8% to 2.0%. These shifts suggested that under extreme acidification (pH ≈ 3.58) and intensified heavy metal mobilization, the selective pressures shifted from nitrogen availability toward metal toxicity, altering the competitive hierarchy among these genera. Overall, the changes at the genus level closely corresponded to those at the class level: the *Gammaproteobacteria* affiliated *Chujaibacter* was the most responsive taxon at the genus level, capable of utilizing NH_4^+ and surviving under low pH conditions, indicating its dominant role in nitrification under urea-treated conditions. Meanwhile, *Sphingomonas* and *norank-f-Acidobacteriaceae-(Subgroup-1)* exhibited contrasting trajectories in response to heavy metal stress and organic matter degradation, respectively. Overall, these genera collectively represent the genus-level community succession and the selective filtering effect of different urea concentrations, pH decline, and metal mobilization on the microbial community.

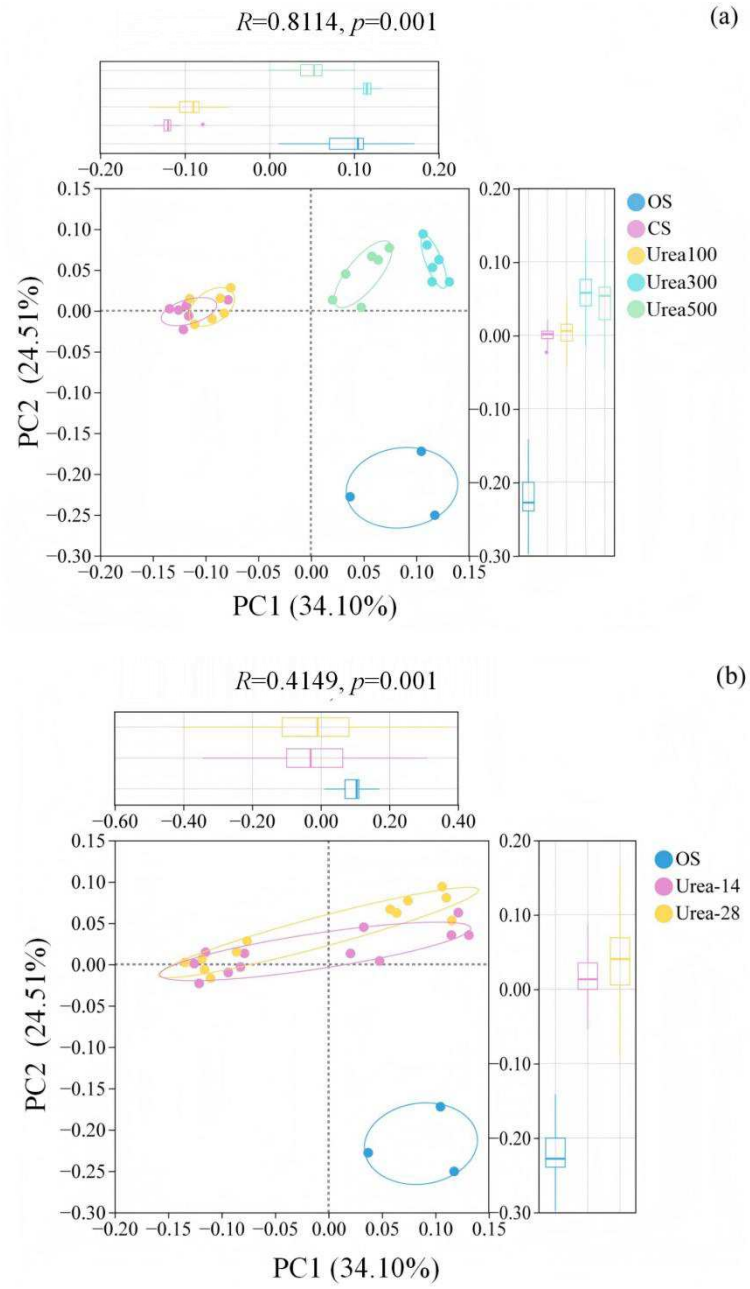


Fig. 5. Principal coordinate analysis (PCoA) of soil microbial community structure at the genus level based on Bray-Curtis distance. (a) PCoA ordination of samples grouped by urea application rate (OS, CS, Urea100, Urea300, and Urea500); (b) PCoA ordination of samples grouped by incubation time (OS, Urea-14, and Urea-28).

The directional successions were further evidenced by PCoA analysis based on Bray-Curtis distance (Fig. 5). As shown in Fig. 5a, the PC1 and PC2 explained 34.10% and 24.51% of the

458 total variation in bacterial community structure, respectively, with a cumulative explanation of
459 58.61%, indicating that the first two principal coordinates effectively captured the
460 compositional differences among treatments. The CS and Urea100 groups largely overlapped
461 in the ordination space, suggesting that low-rate urea addition exerted only a minor effect on
462 overall community structure. In contrast, the Urea300 and Urea500 groups formed distinct and
463 well-separated clusters from each other, and both diverged from the low-rate group along the
464 PC1 axis, indicating that higher urea inputs induced a directional shift in community succession,
465 the magnitude of which intensified with increasing nitrogen addition. Notably, the OS group
466 was clearly separated from all incubated groups along the PC2 axis, reflecting that the
467 incubation conditions themselves imposed a strong directional filtering effect on the soil
468 microbial community. Fig. 5 (b) reveals a different pattern when samples were grouped by
469 incubation time. The Urea-14 and Urea-28 samples largely overlapped in the ordination space
470 without significant separation, yet both were clearly distinct from the OS group, indicating that
471 the major structural reorganization of the community had already occurred by day 14 and
472 subsequently remained relatively stable through day 28.

473 **3.3.3 Functional predictions of soil bacterial communities**

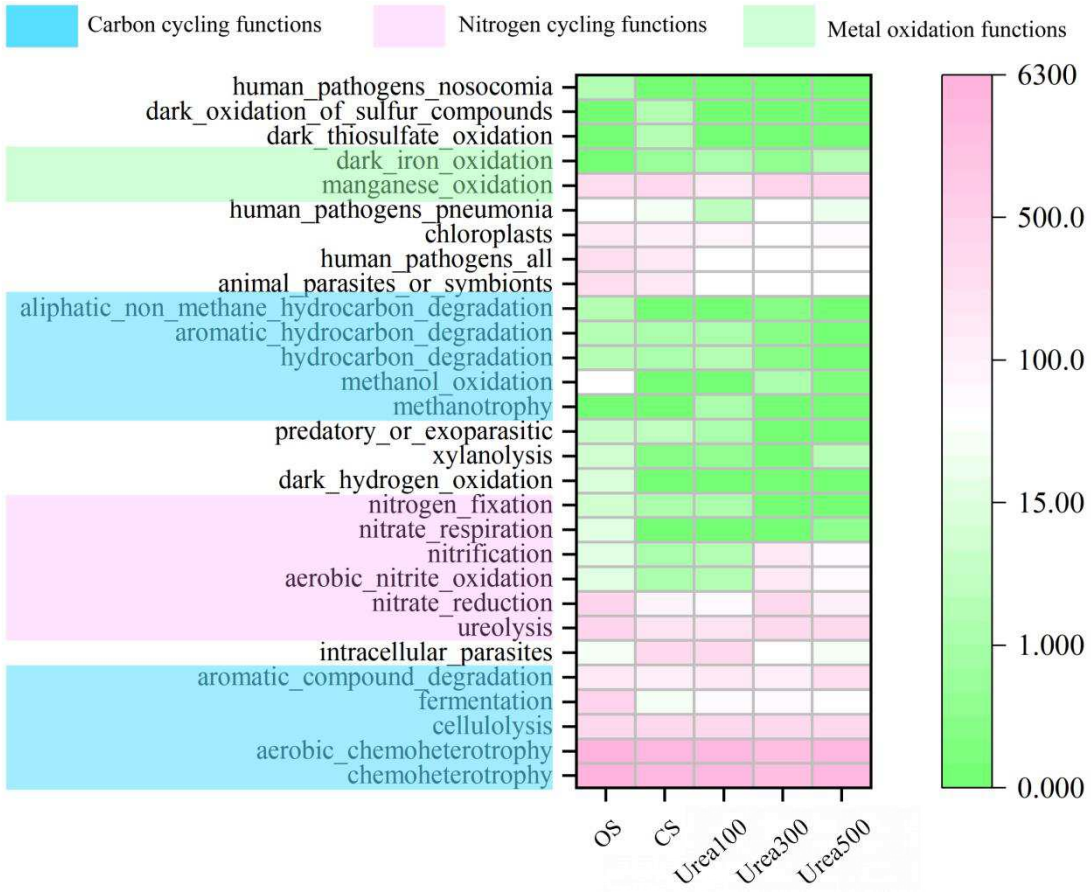


Fig. 6. Heatmap analysis of bacterial functional profiles under different urea application treatments (OS, CS, Urea100, Urea300, and Urea500).

Based on FAPROTAX functional annotation of 16S rRNA amplicon sequencing data, a total of 29 functional groups were identified in this study, involving carbon metabolism, nitrogen cycling, and metal redox processes (Table S3). Among the carbon metabolism functional groups, chemo-heterotrophy and aerobic-chemo-heterotrophy exhibited the highest relative abundances across all treatment groups, representing the dominant components of microbial energy metabolism (Banerjee et al., 2016; Zhu et al., 2024). Notably, the relative abundances of these two genes were 38.5% and 37.4% in Urea300 and 41.0% and 40.3% in Urea500, which were all lower than those in the CS group (42.2% and 43.8%), indicating that high-rate urea application exerted a marked inhibitory effect on carbon cycling functions. Furthermore,

hydrocarbon degradation functions, including hydrocarbon-degradation, aromatic-hydrocarbon-degradation, and aromatic-compound-degradation, were almost completely lost in Urea300 and Urea500, suggesting that urea-indued acidification strongly suppressed this functional guild. Such suppression could severely impair the natural attenuation capacity of soil for petroleum hydrocarbon contaminants; under sustained acidification, this ecosystem service might be entirely lost, posing potential ecological and environmental risks.

Among the nitrogen cycling functional groups, ureolysis increased from 1.2% in the CS group to 3.8% and 3.2% in Urea300 and Urea500, indicating that urea addition stimulated the proliferation and metabolic activation of ureolytic microorganisms. Nitrification increased to 1.8% and 0.9% in Urea300 and Urea500, respectively; similarly, aerobic-nitrite-oxidation showed a consistent increasing trend, further confirming that complete nitrification ($NH_4^+ \rightarrow NO_2^- \rightarrow NO_3^-$) occurred under high urea addition (Bhatti et al., 2017; Jiao et al., 2025). Notably, both functions peaked in Urea300 and declined in Urea500, suggesting that extreme acidification (pH ≈ 3.58) may have partially inhibited the nitrifying community. Nitrate reduction exhibited a synchronous trend with the nitrification functional groups: compared with the CS (0.8%), its relative abundance increased to 2.9% and 1.4% in Urea300 and Urea500, respectively. This coordinated enhancement indicated that nitrate reduction was strengthened alongside nitrification, which could explain the observed patterns in Figs. 1b and 1d, where NH_4^+ peaked and began to decline on day 14 while NO_3^- remained stable, due to the concurrent action of nitrate reduction consuming NO_3^-. However, the relative abundance of nitrogen fixation decreased to nearly zero in Urea300 and Urea500.

This result indicated that the strong environmental stress, particularly the sharp pH decline induced by medium- and high-rate urea addition exceeded the tolerance thresholds of the nitrogen-fixing microbial groups, leading to the complete suppression of this important nitrogen cycling process in the medium- and high-nitrogen treatments.

Among metal oxidation functions, manganese oxidation increased substantially in the Urea300 and Urea500 groups. This process oxidizes soluble Mn^{2+} to insoluble MnO_2 precipitates, and biogenic MnO_2 exhibits strong adsorption capacity for heavy metal ions such as Cd^{2+} and Cu^{2+} (100~200 mg/g; Zhao et al., 2026). Therefore, enhanced manganese oxidation could, to some extent, reduce the bioavailability and migration risk of heavy metals in soil, constituting a microbe-mediated self-detoxification mechanism. Meanwhile, the relative abundance of dark iron oxidation increased continuously with increasing urea application rate, indicating that the substantial release of Fe^{2+} under acidification provided sufficient electron donors for iron-oxidizing microorganisms (Qi et al., 2026), further reinforcing the synergistic immobilization of heavy metals by iron and manganese oxides. The coordinated enhancement of these metal oxidation functions represents an active biogeochemical response of the microbial community to heavy metal stress.

FAPROTAX functional annotation (Fig. 6) showed that the relative abundances of nitrification, aerobic nitrite oxidation, and nitrate reduction all peaked in the Urea300 (133.2, 133.2, and 216.7, respectively), and then declined sharply in Urea500 to 77.3, 77.3, and 128.3, with reductions of 41.9%, 41.9%, and 40.8%, respectively. This functional trend was highly consistent with the population dynamics of the genus *Chujaibacter*, the relative abundance of which reached to 17.9% in Urea300, then fell back to 14.2% in Urea500. This genus,

belonging to *Gammaproteobacteria*, is a key microbial taxon driving enhanced nitrification (Ren et al., 2026). Concurrently, the functional genes encoding chemo-heterotrophy and aerobic chemo-heterotrophy reached their lowest levels in Urea300 and then rebounded significantly in Urea500 (by 26.0% and 27.3%, respectively), paralleling the recovery trend of the genus *Sphingomonas* (Liu et al., 2021; Rousk et al., 2010), which recovered from 2.3% in Urea300 to 3.6% in N500. In addition, aromatic compound degradation also rebounded in Urea500, consistent with the synchronous increase in abundance of genera such as *Sphingomonas* and *Gemmatimonas*. Overall, these data revealed that in the Urea300 treatment, the substantial enrichment of *Gammaproteobacteria* (particularly *Chujaibacter*) and the concurrent decline of *Alphaproteobacteria* jointly explain the anomalous alpha diversity patterns, that Urea300 exhibited lower species richness and poorer evenness than Urea500. Furthermore, the pronounced increases in nitrification, aerobic nitrite oxidation, and nitrate reduction in Urea300 were driven by microorganisms such as *Chujaibacter* (Escalas et al., 2019; Guo et al., 2026; Zhou et al., 2017). This also accounts for the observation in Section 3.1 that Urea300, despite receiving less urea input, achieved NH_4^+ and NO_3^- concentrations comparable to those of Urea500—a phenomenon attributable to the stronger nitrification function in Urea300.

4. Discussion

4.1 Hysteretic response and differential release of heavy metal mobilization

Soil acidification in Chinese farmland has been extensively documented by numerous large-scale surveys and is primarily attributed to excessive nitrogen fertilizer (Tian and Niu, 2015). The nitrification of NH4+ not only drives soil acidification but also promotes the

552 mobilization of heavy metal ions by pH reduction and the concomitant decomposition of
553 organic matter (Jones et al., 2019; Li et al., 2026). In the present study, the soluble
554 concentrations of Fe, Zn, Cd, and Cu generally increased with incubation time; however, the
555 release rates, peak times, and magnitudes of increase varied considerably among elements,
556 implying that the mobilization effect of urea-driven acidification is element-specific across
557 metals. Cu and Fe exhibited higher sensitivity to mobilization, with discernible increases
558 commencing from day 14. By day 28, the Cu concentration in the Urea500 treatment had
559 increased by approximately 0.05 mg/kg relative to the initial value, while Fe increased by about
560 8 mg/kg. In contrast, the mobilization of Cd and Zn displayed a distinct lag, with significant
561 increases occurring only after day 14. This differential temporal pattern may be attributed to the
562 distinct chemical speciation of each metal in the soil solid phase. Cu and Fe are primarily
563 associated with Fe-Mn oxide-bound and organic matter-bound fractions (Hu et al., 2023); the
564 decline in pH preferentially disrupts the adsorption equilibrium on oxide surfaces, facilitating
565 the early desorption of Cu and Fe. By contrast, Cd, is predominantly present in carbonate-bound
566 forms (Liu et al., 2013), the release of which requires a further reduction in pH to achieve
567 substantial desorption (Jiang et al. 2026). Notably, the mobilization of Zn, Cu, and Cd did not
568 reach their respective peaks until day 60, whereas soil pH had already attained its minimum by
569 day 28. This lag effect of approximately one month indicates that the transfer of heavy metals
570 from the solid adsorbed phase to the soluble phase is a multi-step kinetic process. Specifically,
571 the initial pH decline first alters the surface adsorption equilibrium, which is then followed by
572 gradual desorption, dissolution, and diffusion; only after these sequential steps do metal ions
573 enter the soluble phase in substantial quantities (Huang et al., 2015). This hysteresis effect has

574 important implications for practical farmland management: even if soil pH begins to recover
575 after the depletion of urea substrate, the heavy metals already released into the liquid phase will
576 persist at relatively elevated concentrations in the short term. Consequently, their biotoxicity
577 and leaching risks will not be simultaneously eliminated with the natural recovery of pH, posing
578 a sustained environmental threat that warrants careful attention in post-acidification
579 remediation strategies (Chen et al., 2024).

580 **4.2 Bacterial community succession and environmental responses**

581 The response of soil microbial communities to urea addition is a nonlinearly coupled process
582 governed by multiple interacting environmental factors. The present study revealed that the
583 response trajectories of microbial communities under different urea application treatments do
584 not follow a simple linear acidification progression; rather, they exhibited shifts driven by
585 multiple environmental variables including pH, NH_4^+, NO_3^-, and heavy metal ions. The trends
586 in alpha diversity provide direct evidence for this multifactor coupling. In the low-urea
587 treatment (Urea100), NH_4^+ enrichment provided an additional nitrogen source for
588 microorganisms, and alpha diversity slightly recovered compared with the control group,
589 suggesting that moderate urea addition could help maintain community diversity to some extent
590 (Fiedler et al., 2016; Garcia-Gil et al., 2004). In contrast, in the high-urea groups (Urea300 and
591 Urea500), the microbial community did not change simply in proportion to urea application
592 rate, but showed divergent trends in richness and evenness. Nevertheless, alpha diversity alone
593 reflects only overall community-level changes and is insufficient to reveal the differential
594 response trajectories of distinct functional groups within the community.

595 Combining the community composition data (Fig. 4) with the functional predictions (Fig. 6),

it further elucidated the specific pathways of functional community coupling. FAPROTAX functional prediction showed that nitrification, aerobic nitrite oxidation, and nitrate reduction all peaked in Urea300 and then declined in Urea500. This functional trajectory of first increasing and then decreasing was highly coupled with the population dynamics of *Gammaproteobacteria* and its representative genus *Chujaibacter*—indicating that this genus is the direct microbial carrier of enhanced nitrification. Meanwhile, chemo-heterotrophy and aerobic-chemo-heterotrophy reached their lowest levels in Urea300 (2916.8 and 2834.5) and then rebounded by about 26.0% in Urea500, a trend consistent with the changes in *Alphaproteobacteria* and the genus *Sphingomonas*. All carbon-cycling functions and their associated microorganisms were inhibited during incubation.

In summary, there is a bidirectional feedback regulation mechanism between the microbial community and the soil environment. On the one hand, the H^+ and NH_4^+ released by urea hydrolysis-nitrification select for acid-tolerant nitrifying communities dominated by *Gammaproteobacteria*, which continue to drive nitrification, lower pH, and promote heavy metal mobilization; on the other hand, the overall strong acidic environment and the accumulation of heavy metal (especially Cu and Cd) inhibit the activity of nitrifying and carbon-cycling microbial groups, while providing opportunities for heavy-metal-tolerant taxa to develop. However, in the Urea300 treatment, the nitrifying community was overly active, leading to poorer richness and evenness of the community.

5. Conclusion

In this study, we integrated soil physicochemical analysis, heavy metal mobilization monitoring, 16S rRNA amplicon sequencing, and FAPROTAX functional prediction to

elucidate the response patterns of soil properties, metal mobility, and microbial communities to gradual urea inputs in a wheat-peanut rotation system of the Nanyang Basin, China.

Urea addition induced dose-dependent acidification coupled with marked shifts in inorganic nitrogen speciation. Soil pH declined to its minimum on day 28, with reductions increasing with application rate (23.7%, 25.2%, and 26.2% for Urea100, Urea300, and Urea500, respectively). Recovery by day 60 was limited and negatively correlated with urea input, indicating weakened acid-buffering capacity under high nitrogen loading. NH_4^+-N peaked on day 14 and remained elevated at day 60 in high-N treatments, suggesting constrained nitrification. A transient NO_2^--N accumulation on day 28 coincided with the pH minimum, confirming nitrification as the dominant proton-producing pathway, while NO_3^--N increased 4.7 ~ 5.8-fold and stabilized thereafter.

Heavy metal mobilization exhibited a pronounced hysteretic response that Cd, Cu, and Zn mobilization peaked on day 60—a lag of approximately one month after pH reached its minimum. Although all metals remained below GB 15618-2018 thresholds, this hysteresis decouples metal toxicity from pH recovery, leaving a sustained environmental risk.

Urea application altered bacterial community structure and function. Low urea addition (Urea100) had minimal effects, whereas Urea300 triggered drastic changes reorganization (nitrification and manganese oxidation increased; aerobic chemo-heterotrophy halved; nitrogen fixation and hydrocarbon degradation nearly eliminated). In Urea500, partial recovery of nitrification and chemo-heterotrophy, together with peak aromatic degradation, yielded greater community stability than Urea300, reflecting functional rebalancing rather than a simple dose-dependent decline. Functional shifts were tightly coupled with taxonomic reorganization.

Gammaproteobacteria and its representative genus *Chujaibacter* were primary carriers of enhanced nitrification, peaking in Urea300, while *Alphaproteobacteria* and *Sphingomonas* exhibited inverse trends, recovering in Urea500 alongside chemoheterotrophic functions, indicating divergent ecological strategies among lineages under acidification stress.

These findings inform nitrogen management in intensive agriculture. Given the nonlinear community responses and hysteretic metal mobilization, single urea applications should be controlled below 300 kg N/ha with intervals of no less than 60 days. In high-risk regions, liming or nitrification inhibitors should be considered to balance fertilizer efficiency with long-term soil ecological safety. Future work should quantify alternative nitrification pathways under extreme acidification (pH < 4.0), validate thresholds through long-term field trials, and apply co-occurrence network analysis to predict ecosystem functional resilience under anthropogenic nitrogen inputs.

CRediT authorship contribution statement

Lu Xia: Investigation, Methodology, Writing- original draft, Data curation. **Tao Liu:** Investigation, Methodology, Writing- Reviewing and Editing, Data curation. **Bin Li** : Writing- Reviewing and Editing. **Jie Chen:** Writing- Reviewing and Editing, Data curation. **Mengjie Qin:** Writing- Reviewing and Editing. **Haoahao Cui:** Funding acquisition, Supervision, Writing- Reviewing and Editing. **Fengxin Kang:** Funding acquisition, Supervision, Writing- Reviewing and Editing.

Acknowledgements

This work was financially supported by the Open Project Program of the Shan-dong Provincial Lunan Geo-engineering Exploration Institute (grant number LNY202606) and Geological survey project of China Geological Survey (number DD20230700905). Sincere gratitude is also expressed to the reviewers for their many helpful and constructive comments.

Data availability

Data will be made available on request.

References

Banerjee, S., Kirkby, C.A., Schmutter, D., Bissett, A., Kirkegaard, J.A., Richardson, A.E., 2016. Network analysis reveals functional redundancy and keystone taxa amongst bacterial and fungal communities during organic matter decomposition in an arable soil. Soil Biol. Biochem. 97, 188–198. https://doi.org/10.1016/j.soilbio.2016.03.017

Bartkowska-Bekasiewicz, A., Mieczan, T., Toporowska, M., 2026. Effect of cyanobacteria metabolites on bacterial consortia in peatbog ecosystems: Metagenomic analysis. J. Nat. Conserv. 93, 127355. https://doi.org/10.1016/j.jnc.2026.127355

Bhatti, A.A., Haq, S., Bhat, R.A., 2017. Actinomycetes benefaction role in soil and plant health. Microb. Pathog. 111, 458–467. https://doi.org/10.1016/j.micpath.2017.09.036

Chen, Z., Liu, Q., Chen, D., Wu, Y., Hamid, Y., Lin, Q., Zhang, S., Feng, Y., He, Z., Yin, X., Yang, X., 2024. Enhancing the phytoextraction efficiency of heavy metals in acidic and alkaline soils by Sedum alfredii Hance: A study on the synergistic effect of plant growth regulator and plant growth-promoting bacteria. Sci. Total Environ. 932, 173029. https://doi.org/10.1016/j.scitotenv.2024.173029

Dai, Z., Zhang, X., Tang, C., Muhammad, N., Wu, J., Brookes, P.C., Xu, J., 2017. Potential role of biochars in decreasing soil acidification—a critical review. Sci. Total Environ. 581–582, 601–611. https://doi.org/10.1016/j.scitotenv.2016.12.169

Dong, Y., Yang, J.-L., Zhao, X.-R., Yang, S.-H., Mulder, J., Dorsch, P., Peng, X.-H., Zhang, G.-L., 2022. Soil acidification and loss of base cations in a subtropical agricultural watershed. Sci. Total Environ. 827, 154338. https://doi.org/10.1016/j.scitotenv.2022.154338

Dror, I., Yaron, B., Berkowitz, B., 2017. Microchemical contaminants as forming agents of anthropogenic

691 soils. Ambio 46, 109–120. https://doi.org/10.1007/s13280-016-0804-7
692 Duan, Y., Zhang, J., Petropoulos, E., Zhao, J., Jia, R., Wu, F., Chen, Y., Wang, L., Wang, X., Li, Y., et al.,
693 2025. Soil acidification destabilizes terrestrial ecosystems via decoupling soil microbiome. Glob.
694 Change Biol. 31, e70174. https://doi.org/10.1111/gcb.70174
695 Escalas, A., Hale, L., Voordeckers, J.W., Yang, Y., Firestone, M.K., Alvarez-Cohen, L., Zhou, J., 2019.
696 Microbial functional diversity: from concepts to applications. Ecol. Evol. 9, 12000–12016.
697 https://doi.org/10.1002/ece3.5670
698 Fiedler, S.R., Leinweber, P., Jurasinski, G., Eckhardt, K.-U., Glatzel, S., 2016. Tillage-induced short-term
699 soil organic matter turnover and respiration. Soil 2, 475–486. https://doi.org/10.5194/soil-2-475-
700 2016
701 Fierer, N., Jackson, R.B., 2006. The diversity and biogeography of soil bacterial communities. Proc. Natl.
702 Acad. Sci. USA 103, 626–631. https://doi.org/10.1073/pnas.0507535103
703 Food and Agriculture Organization of the United Nations (FAO) and Intergovernmental Technical Panel on
704 Soils (ITPS), 2015. Status of the World's Soil Resources (SWSR): Main Report. FAO.
705 Frey, S.D., Knorr, M., Parrent, J.L., Simpson, R.T., 2004. Chronic nitrogen enrichment affects the structure
706 and function of the soil microbial community in temperate hardwood and pine forests. For. Ecol.
707 Manag. 196, 159–171. https://doi.org/10.1016/j.foreco.2004.03.018
708 Garcia-Gil, J.C., Ceppi, S.B., Velasco, M.I., Polo, A., Senesi, N., 2004. Long-term effects of amendment with
709 municipal solid waste compost on the elemental and acidic functional group composition and pH-
710 buffer capacity of soil humic acids. Geoderma 121, 135–142.
711 https://doi.org/10.1016/j.geoderma.2003.11.004
712 Guo, J.H., Liu, X.J., Zhang, Y., Shen, J.L., Han, W.X., Zhang, W.F., Christie, P., Goulding, K.W.T., Vitousek,

P.M., Zhang, F.S., 2010. Significant acidification in major Chinese croplands. Science 327, 1008–1010. https://doi.org/10.1126/science.1182570

Guo, T., Qi, J., Liu, H., Cao, Y., Ge, Q., Liang, X., Jiang, Y., Jiang, Q., 2026. Metabolic landscape of panax ginseng under forest cultivation across multiple growth years: Associations with soil microbiota and regulatory networks governing ginsenoside accumulation. Ind. Crops Prod. 239, 122542. https://doi.org/10.1016/j.indcrop.2026.122542

Guo, Z., Fang, J., He, J., et al., 2026. Season-dependent combined effects of nitrogen deposition and precipitation change on soil microbial communities and functions in a subtropical forest. Biol. Fertil. Soils 62, 367–382. https://doi.org/10.1007/s00374-025-01940-2

Holland, J.E., White, P.J., Glendining, M.J., Goulding, K.W.T., McGrath, S.P., 2019. Yield responses of arable crops to liming—an evaluation of relationships between yields and soil pH from a long-term liming experiment. Eur. J. Agron. 105, 176–188. https://doi.org/10.1016/j.eja.2019.02.016

Hu, X., Qu, C., Han, Y., Sun, P., Cai, P., Chen, W., Huang, Q., 2023. Elevated temperature induces contrasting transformation of exogenous copper to soil solution and solid phases in an arable soil. Ecotoxicol. Environ. Saf. 255, 114744. https://doi.org/10.1016/j.ecoenv.2023.114744

Huang, P., Zhang, J., Xin, X., Zhu, A., Zhang, C., Ma, D., Zhu, Q., Yang, S., Wu, S., 2015. Proton accumulation accelerated by heavy chemical nitrogen fertilization and its long-term impact on the acidification rate in a typical arable soil in the Huang-Huai-Hai Plain. J. Integr. Agric. 14, 148–157. https://doi.org/10.1016/S2095-3119(14)60750-4

ISO 10390:2024. Soil, treated biowaste, soil and waste — Determination of pH. International Organization for Standardization, Geneva, Switzerland.

Jiang, Y., Lu, P., Ye, J., Ye, L., Qin, Q., Sun, Y., Yang, S., Wang, J., Jiang, X., Hu, X., Xue, Y., Sun, L., 2026.

Regulation of heavy metal migration by soil colloids under the influence of organic fertilizers. J. Environ. Chem. Eng. 14, 123435. https://doi.org/10.1016/j.jece.2026.123435

Jiao, H., Xu, M., Ji, J., Wang, Y., Zhang, Y., Su, B., Zhang, H., Gao, C., 2025. Bacterial and fungal diversity, community composition, functional groups, and co-occurrence network succession in dryland and paddy soils along a 3000-year chronosequence. CATENA 248, 108582. https://doi.org/10.1016/j.catena.2024.108582

Jones, D.L., Cooledge, E.C., Hoyle, F.C., Griffiths, R.I., Murphy, D.V., 2019. pH and exchangeable aluminum are major regulators of microbial energy flow and carbon use efficiency in soil microbial communities. Soil Biol. Biochem. 138, 107584. https://doi.org/10.1016/j.soilbio.2019.107584

Kraamwinkel, C.T., Beaulieu, A., Dias, T., Howison, R.A., 2021. Planetary limits to soil degradation. Commun. Earth Environ. 2, 249. https://doi.org/10.1038/s43247-021-00323-3

Kyveryga, P.M., Blackmer, A.M., Ellsworth, J.W., Isla, R., 2004. Soil pH effects on nitrification of fall-applied anhydrous ammonia. Soil Sci. Soc. Am. J. 68, 545–551. https://doi.org/10.2136/sssaj2004.5450

Li, L., Dong, M., He, L., Chen, H., Yu, M., Gustave, W., Li, B., Zhang, X., He, F., 2026. Interactions between lake dissolved organic matter and heavy metals: implications for ecological risk assessment. Environ. Rev. 34, 1–17. https://doi.org/10.1139/er-2025-0181

Liu, X., Zhang, Y., Han, W., Tang, A., Shen, J., Cui, Z., Vitousek, P., Erisman, J.W., Goulding, K., Christie, P., et al., 2013. Enhanced nitrogen deposition over China. Nature 494, 459–462. https://doi.org/10.1038/nature11917

Liu, Z., Wei, H., Zhang, J., Saleem, M., He, Y., Zhong, J., Ma, R., 2021. Seasonality regulates the effects of acid rain on microbial community in a subtropical agricultural soil of southern China. Ecotoxicol.

Environ. Saf. 224, 112681. https://doi.org/10.1016/j.ecoenv.2021.112681

Llado, S., Benada, O., Cajthaml, T., Baldrian, P., Garcia-Fraile, P., 2016. Silvibacterium bohemicum gen. nov. sp. nov., an acidobacterium isolated from coniferous soil in the Bohemian Forest National Park. Syst. Appl. Microbiol. 39, 14–19. https://doi.org/10.1016/j.syapm.2015.11.001

Meng, C., Tian, D., Zeng, H., Li, Z., Yi, C., Niu, S., 2019. Global soil acidification impacts on belowground processes. Environ. Res. Lett. 14, 074003. https://doi.org/10.1088/1748-9326/ab239c

Ministry of Ecology and Environment of the People's Republic of China, State Administration for Market Regulation, 2018. Soil environmental quality—Risk control standard for soil contamination of agricultural land (trial). GB 15618-2018. Beijing: China Environmental Publishing Group.

Morrison, E.W., Frey, S.D., Sadowsky, J.J., Van Diepen, L.T.A., Thomas, W.K., Pringle, A., 2016. Chronic nitrogen additions fundamentally restructure the soil fungal community in a temperate forest. Fungal Ecol. 23, 48–57. https://doi.org/10.1016/j.funeco.2016.05.011

Niepceron, M., Martin-Laurent, F., Crampon, M., Portet-Koltalo, F., Akpa-Vinceslas, M., Legras, M., Bru, D., Bureau, F., Bodilis, J., 2013. GammaProteobacteria as a potential bioindicator of a multiple contamination by polycyclic aromatic hydrocarbons (PAHs) in agricultural soils. Environ. Pollut. 180, 199–205. https://doi.org/10.1016/j.envpol.2013.05.040

Qi, Z., Wang, L., Shi, Y., Guan, R., Wang, L., Zhang, Y., 2026. Algae-bacteria alleviate GHG emissions by oxidation barrier, carbon-iron cycle, microbial community restructuring in Northeast China Mollisol paddy fields. Agric. Ecosyst. Environ. 408, 110469. https://doi.org/10.1016/j.agee.2026.110469

Qu, X., Li, X., Bardgett, R.D., Kuzyakov, Y., Revillini, D., Sonne, C., Xia, C., Ruan, H., Liu, Y., Cao, F., et al., 2024. Deforestation impacts soil biodiversity and ecosystem services worldwide. Proc. Natl. Acad. Sci. USA 121, e2318475121. https://doi.org/10.1073/pnas.2318475121

Ren, J., Gao, J., Wang, F., Li, X., Cao, S., Shon, H.K., 2026. Biological enzyme-enhanced hydrolysis and nitrification for nutrient recovery from hormone-extracted urine. Desalination 629, 120161. https://doi.org/10.1016/j.desal.2026.120161

Ren, T., Xue, Y., Miao, T., Liu, K., Zhang, W., Cai, A., 2026. Manure increases temperature sensitivity of soil organic carbon by increasing soil Alphaproteobacteria, phenols, and pH and decreasing soil esters. J. Integr. Agric. 25, 2993–3005. https://doi.org/10.1016/j.jia.2025.09.021

Rousk, J., Baath, E., Brookes, P.C., Lauber, C.L., Lozupone, C., Caporaso, J.G., Knight, R., Fierer, N., 2010. Soil bacterial and fungal communities across a pH gradient in an arable soil. ISME J. 4, 1340–1351. https://doi.org/10.1038/ismej.2010.58

Shen, C., Xiong, J., Zhang, H., Feng, Y., Lin, X., Li, X., Liang, W., Chu, H., 2013. Soil pH drives the spatial distribution of bacterial communities along elevation on Changbai Mountain. Soil Biol. Biochem. 57, 204–211. https://doi.org/10.1016/j.soilbio.2012.07.013

Tian, D., Niu, S., 2015. A global analysis of soil acidification caused by nitrogen addition. Environ. Res. Lett. 10, 024019. https://doi.org/10.1088/1748-9326/10/2/024019

Van Vuuren, D.P., Doelman, J.C., Schmidt Tagomori, I., Beusen, A.H.W., Cornell, S.E., Rockstrom, J., Schipper, A.M., Stehfest, E., Ambrosio, G., van den Berg, M., et al., 2025. Exploring pathways for world development within planetary boundaries. Nature 641, 910–916. https://doi.org/10.1038/s41586-025-08928-w

Wang, S., Li, X., Zhang, L., Zhang, W., Xu, L., Qiu, L., Chen, G., Hu, J., Zhou, S., Tu, L., 2026. Re-evaluating forest carbon sinks under nitrogen deposition: Acidification drives passive carbon accumulation via decoupling microbial manganese oxidation. J. Environ. Manage. 414, 130573. https://doi.org/10.1016/j.jenvman.2026.130573

Wang, T., Cao, X., Chen, M., Lou, Y., Wang, H., Yang, Q., Pan, H., Zhuge, Y., 2022. Effects of soil acidification on bacterial and fungal communities in the Jiaodong Peninsula, northern China. Agronomy 12, 927. https://doi.org/10.3390/agronomy12040927

Wang, X., Feng, J., Ao, G., Qin, W., Han, M., Shen, Y., Liu, M., Chen, Y., Zhu, B., 2023. Globally nitrogen addition alters soil microbial community structure, but has minor effects on soil microbial diversity and richness. Soil Biol. Biochem. 179, 108982. https://doi.org/10.1016/j.soilbio.2023.108982

Yang, Y., Chen, L., Liu, T., Wang, E., Tan, Z., Li, Z., 2025. Efficient ammonia oxidation by Pseudomonas citronellolis strain YN-21 under strongly acidic conditions: Performance and mechanism. Bioresour. Technol. 417, 131887. https://doi.org/10.1016/j.biortech.2024.131887

Yang, Y., Cheng, H., Gao, H., An, S., 2020. Response and driving factors of soil microbial diversity related to global nitrogen addition. Land Degrad. Dev. 31, 190–204. https://doi.org/10.1002/ldr.3439

Zhao, W., Cai, C., Zhou, J., Chu, Z., 2026. Manganese mineralization driven by microbial methane oxidation coupled with reduction of Mn oxides. J. Geochem. Explor. 290, 108171. https://doi.org/10.1016/j.gexplo.2026.108171

Zhou, X., Guo, Z., Chen, C., Jia, Z., 2017. Soil microbial community structure and diversity are largely influenced by soil pH and nutrient quality in 78-year-old tree plantations. Biogeosciences 14, 2101–2111. https://doi.org/10.5194/bg-14-2101-2017

Zhu, L., Wang, L., Zhang, J., Xu, Y., Li, X., Zhang, M., Ma, B., 2024. Comparison of characteristics of biochar modified by earthworm and potassium permanganate. Environ. Technol. Innov. 35, 103733. https://doi.org/10.1016/j.eti.2024.103733